Chem

CellPress

Article

Observation of a potential-dependent switch of water-oxidation mechanism on Co-oxide-based catalysts

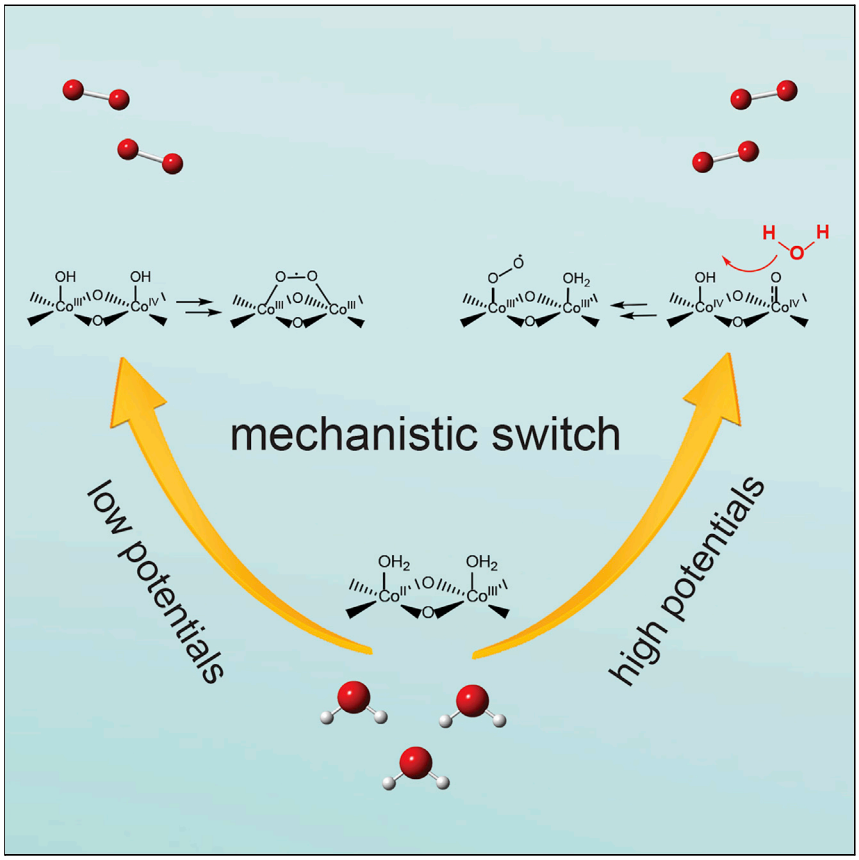

The O–O bond formation is a key elementary step of the water-oxidation reaction, of which the dependence on the applied potential remains ambiguous. Using water-in-salt electrolyte, we systematically tuned the water activity and probed the mechanism as a function of applied potentials. We found that the mechanism is sensitive to the applied potential. The O–O bond forms via an intramolecular oxygen coupling mechanism at low potentials, whereas it proceeds through a water nucleophilic attack mechanism at high potentials.

Chaochao Lang, Jingyi Li, Ke R. Yang, ..., Victor S. Batista, Matthias M. Waegele, Dunwei Wang

victor.batista@yale.edu (V.S.B.)
waegele@bc.edu (M.M.W.)
dunwei.wang@bc.edu (D.W.)

Highlights

A key superoxo intermediate for water oxidation was detected with SEIRAS-ATR

A potential-dependent O–O bond-formation mechanism is revealed

The intramolecular oxygen coupling mechanism dominates at low potentials

The water nucleophilic attack mechanism prevails at high potentials

Lang et al., Chem 7, 2101–2117
August 12, 2021
https://doi.org/10.1016/j.chempr.2021.03.015

Chem

CellPress

Article

Observation of a potential-dependent switch of water-oxidation mechanism on Co-oxide-based catalysts

Chaochao Lang,[1,3] Jingyi Li,[1,3] Ke R. Yang,[2,3] Yuanxing Wang,[1,3] Da He,[1] James E. Thorne,[1] Seth Croslow,[1] Qi Dong,[1] Yanyan Zhao,[1] Gabriela Prostko,[1] Gary W. Brudvig,[2] Victor S. Batista,[2,*] Matthias M. Waegele,[1,*] and Dunwei Wang[1,4,*]

SUMMARY

O–O bond formation is a key elementary step of the water-oxidation reaction. However, it is still unclear how the mechanism of O–O coupling depends on the applied electrode potential. Herein, using water-in-salt electrolytes, we systematically altered the water activity, which enabled us to probe the O–O bond-forming mechanism on heterogeneous Co-based catalysts as a function of applied potential. We discovered that the water-oxidation mechanism is sensitive to the applied potential: At relatively low driving force, the reaction proceeds through an intramolecular oxygen coupling mechanism, whereas the water nucleophilic attack mechanism prevails at high driving force. The observed mechanistic switch has major implications for the understanding and control of the water-oxidation reaction on heterogeneous catalysts.

INTRODUCTION

Intense research on the water-oxidation catalyst (WOC) center in photosystem II (PSII) over the last decades has revealed deep insights on the mechanisms by which nature liberates electrons and protons from H_2O, two critical ingredients for downstream reactions such as CO_2 reduction and N_2 fixation.[1,2] This knowledge has propelled research on using molecular catalysts to oxidize water, and impressive progress has been made in terms of catalyst performance as measured by turn-over frequencies (TOFs) and turn-over numbers.[3,4] From a technological development perspective, there is a strong incentive to perform the reaction on heterogeneous catalysts, especially on those of low-cost and outstanding stability. Indeed, recent years have witnessed a surge of such research activities.[5–11] Despite the apparent variety of these catalysts, they share important commonalities in the chemical mechanisms. For instance, it is generally believed that the reaction proceeds through a series of proton-coupled electron transfer steps that lead to the formation of M=O (where M represents an active metal center) intermediates.[12,13] It is also agreed upon that the subsequent O–O bond formation is of critical importance to the overall reaction.[14] However, the details of the O–O formation and the subsequent steps have been the subject of diverging views. At least two possible pathways have been proposed and supported.[15–18] One involves direct nucleophilic attack of water, followed by O_2 release and regeneration of the catalyst. In the literature, this mechanism is referred to as water nucleophilic attack (WNA) (Figure 1, right pathway).[4,15] The other involves the coupling of two metal-oxo intermediates followed by O_2 release, which is referred to as intramolecular oxygen coupling (IMOC) (Figure 1, left pathway).[15]

The bigger picture

As the first step in natural photosynthesis, the oxidation of water is of paramount importance. It liberates electrons and protons that are required for downstream reactions such as CO_2 and N_2 reduction. Substantial research efforts have been devoted to understanding and, ultimately, performing this reaction at high efficiency with low-cost, long-lasting catalysts. Exciting progress notwithstanding, much remains poorly understood about the reaction, especially when it is performed on heterogeneous catalysts. A key elementary step of the water-oxidation reaction is the formation of the O–O bond. Herein, we report a potential-induced switch of the O–O bond-forming mechanism on Co-oxide-based catalysts. This mechanistic insight is expected to help advance the design of efficient water-oxidation catalysts.

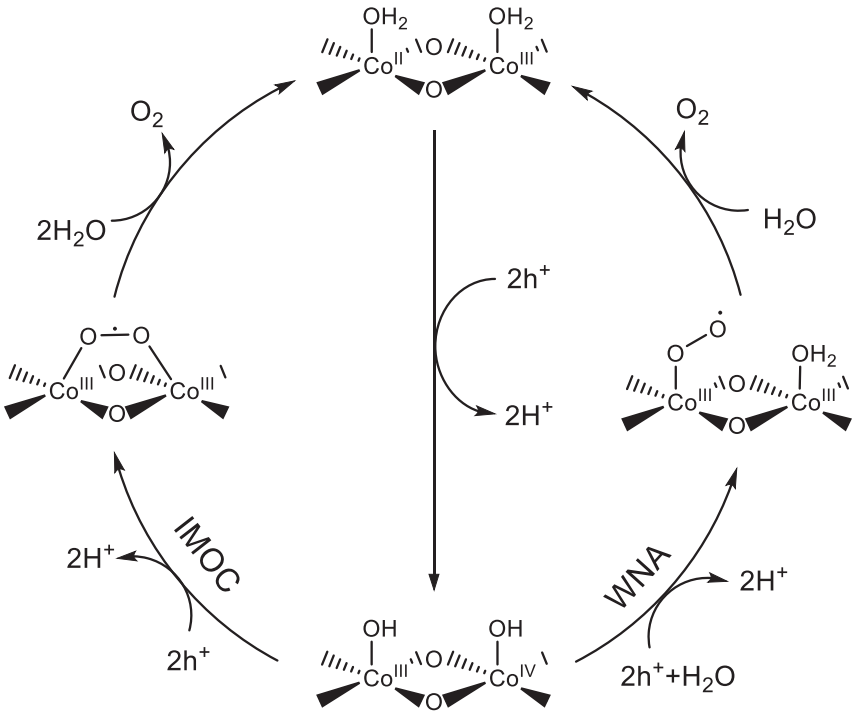

Figure 1. Proposed water-oxidation mechanisms by heterogeneous Co phosphate (Co–Pi) catalysts

Two possibilities have been proposed, the intramolecular oxygen coupling pathway (IMOC, left) and the water nucleophilic attack route (WNA, right).

For Ir- and Ru-based molecular catalysts, density-functional theory (DFT) calculations predicted that the IMOC pathway dominates at low overpotentials, whereas the WNA pathway becomes accessible at higher overpotentials.[17,19] The two pathways were also predicted to be competitive on a heterogenized dinuclear Ir oxide cluster.[17] With optical pump-probe spectroscopy, Cuk et al.[18] monitored the microsecond decay of oxyl (Ti–O•) and bridge (Ti–O•–Ti) intermediates on $SrTiO_3$ photoelectrodes. They found that the two species decay with distinct reaction rates on a microsecond timescale. It was suggested that Ti–O•'s convert to Ti–O–O–Ti by dimerization (IMOC pathway) and Ti–O•–Ti converts to Ti–OOH by nucleophilic attack of water (WNA pathway). Furthermore, it was found that the relative predominance of the two pathways was controlled by the ionic strength of the electrolyte, with the WNA pathway dominating at low ionic strength. However, how the relative predominance of these mechanisms depends on the applied electrode potential has not been investigated in experiments. Herein, we address this central question.

Inspiration on how to further this understanding could be drawn from progress made in molecular WOC-based studies. To discern different pathways for the water-oxidation reaction by molecular catalysts, researchers have resorted to a strategy of correlating the reaction rate with the catalyst concentrations.[4] With the help of additional experiments such as isotope labeling, significant knowledge has been gained.[20–22] However, similar approaches are challenging to implement for heterogeneous catalysts, because the active sites, including their structures and densities, are often poorly defined on a heterogeneous catalyst. The challenge could be circumvented using clever experimental designs. For instance, Durrant et al.[23] have identified a change of reaction orders relative to the hole concentration from the first to the third

[1]Department of Chemistry, Merkert Chemistry Center, Boston College, Chestnut Hill, MA 02467, USA

[2]Yale Energy Sciences Institute and Department of Chemistry, Yale University, New Haven, CT 06520, USA

[3]These authors contributed equally

[4]Lead contact

*Correspondence:
victor.batista@yale.edu (V.S.B.),
waegele@bc.edu (M.M.W.),
dunwei.wang@bc.edu (D.W.)

https://doi.org/10.1016/j.chempr.2021.03.015

order on Fe_2O_3 using photoinduced absorption spectroscopy. Frei et al.[13] have succeeded in observing both the metal-oxo and superoxo species, using an infrared spectroscopy (IR) technique. In both studies, different reaction mechanisms were proposed for different light intensities. Nevertheless, owing to the lack of detailed information on the active centers, particularly their density under different conditions, it remains difficult to directly corroborate these early observations for an unambiguous understanding of water oxidation on heterogeneous catalysts. Although it is possible to address this challenge by synthesizing heterogeneous catalysts with well-defined active centers, as has been demonstrated recently by others and us,[24,25] the catalyst library remains limited, and significant work is needed before the values of such catalysts can be materialized. An alternative approach is to study how the reaction kinetics changes as a function of water activity, which is the main strategy for this present work.

To appreciate the significance of this strategy, it helps to examine the proposed WNA and IMOC pathways on a heterogeneous Co phosphate (Co–Pi) catalyst (Figure 1). Previous studies have suggested that the initial electron/proton transfer steps (vertical arrow in the center) are fast in comparison with the O–O formation. Therefore, these steps are quasi-equilibrated, whereas O–O formation limits the rate of the reaction. From the oxidized state of the catalyst shown on the bottom of the scheme, the water-oxidation process can proceed through two distinct pathways: the WNA pathway involves a water molecule within the electric double layer in the rate-determining O–O forming step (right arrow). By contrast, the IMOC pathway only involves surface species in the rate-determining step (RDS) (left arrow). On the basis of this simplified mechanistic picture, the water-oxidation reaction is expected to be (pseudo) first order in the water activity when proceeding through the WNA pathway, whereas it is (pseudo) zeroth order when proceeding through the IMOC pathway. This simplified view assumes that the change in the water activity does not significantly affect the positions of the quasi-equilibria before the presumed RDS of O–O bond formation, as discussed later. Therefore, it is possible to discern the reaction mechanisms even without detailed knowledge of the active centers by altering the water activity, which has not been investigated previously.

The problem is now reduced to how to alter water activity in a water-oxidation reaction. Indeed, most previous studies on this subject have treated water as a substrate of invariant activity, such that it was excluded in most kinetic considerations.[26,27] Only recently did we see advances where the water activity could be suppressed significantly in aqueous solutions.[28–30] The so-called "water-in-salt" electrolyte containing high concentrations of salts (e.g., up to 21 m [mole per kg of H_2O]) represents one such system. The strong solvation effect of the high-concentration ions renders its H_2O behaviors drastically different from those in bulk H_2O. It becomes possible to perform water-oxidation reactions in an aqueous system where the water activity is no longer unity. Therefore, we are offered an opportunity to test the hypothesis proposed in the previous paragraph. That is, we expect a different sensitivity of the kinetics on the water activity for different mechanisms.

To prove this concept, we have chosen Co-oxide-based catalysts as a study platform because they represent a class of most studied heterogeneous WOCs, with Co–Pi receiving arguably the most attention. A broad knowledge base has already been generated.[15,27,31–36] For example, the coordination environment of Co has been identified by a suite of spectroscopic techniques.[34] That the O–O formation is the RDS has been supported by numerous studies.[15,27,31,32,35,36] Both WNA and IMOC mechanisms have been proposed and supported by either experimental or

computational studies for this catalyst.[15,32,35–39] Herein, we report the new observation of a switch from the IMOC pathway at low applied potentials to the WNA mechanism at high applied potentials.

RESULTS AND DISCUSSION

Detection of water-oxidation intermediates

Previous studies have shown that various implementations of infrared and surface-enhanced Raman spectroscopies are powerful probes of water-oxidation intermediates.[12,13,18,40–48] To examine the mechanistic proposal (Figure 1), we employed surface-enhanced infrared absorption spectroscopy (SEIRAS) in the attenuated total reflection (ATR) geometry. In SEIRAS-ATR, the surface plasmon resonance of rough metal films locally enhances the evanescent field, rendering the technique sensitive to sub-monolayers of species adsorbed on the electrode.[49] With this work, we establish SEIRAS-ATR in the Kretschmann configuration as a tool for probing water-oxidation intermediates on metal oxide catalysts. For this purpose, we first electrochemically deposited a thin layer of $CoO_x(OH)_y$[31] onto a chemically deposited Au thin film ($CoO_x(OH)_y$-Au)[50] on a micro-machined Si-ATR crystal,[51] which affords high infrared transparency below 1,200 cm^{-1}. A scheme of the setup is shown in Figure S1 in the supplemental information. For SEIRAS-ATR, $CoO_x(OH)_y$ instead of Co–Pi was employed as the prototypical catalyst because the latter would greatly complicate the interpretation of the IR spectra in the region around approximately 1,000 cm^{-1} owing to the phosphate anion and its response to the applied potentials. As will be discussed in detail later in this work, the electrochemical behaviors of $CoO_x(OH)_y$ are comparable with Co–Pi. It also features structurally similar active sites and the same cobalt oxidation states under water-oxidation conditions as Co–Pi.[31,52] The $CoO_x(OH)_y$-Au film exhibits a large activity for water oxidation in comparison with the Au substrate (Figure S2).

Figure 2 shows the steady-state spectra of the $CoO_x(OH)_y$-Au electrode in 0.1 M potassium phosphate (KPi) in D_2O, H_2O, and $H_2{}^{18}O$. The absorbance was calculated according to absorbance = $-\log(S/R)$, where S and R refer to the sample and reference spectra, respectively, taken at 2.21 and 1.61 V. Unless otherwise noted, all potentials in this work are relative to the reversible hydrogen electrode. The spectrum in the D_2O-based electrolyte exhibited a band centered at 1,014 cm^{-1} (at 2.21 V) (Figure 2A). The intensity of this band increased with increasing applied potential (Figure S3), suggesting that it is caused by a water-oxidation intermediate. To assign the band to a water-oxidation intermediate, we performed the following control experiments: First, to exclude the possibility that the band (1,014 cm^{-1}) arises from a phosphate species in solution, we confirmed that the band also appears when the electrolyte is 0.1 M KCl in D_2O and in H_2O (Figure S4). Second, the band is absent on an Au electrode without the $CoO_x(OH)_y$ film (Figure S4).

These observations strongly suggest that the band centered at 1,014 cm^{-1} is a water-oxidation intermediate on $CoO_x(OH)_y$-Au. According to the proposed mechanism, this spectral feature can be associated with either Co–O–O$^{\bullet}$–Co from the IMOC pathway or Co–O–O$^{\bullet}$ or Co–O–OH from the WNA pathway (Figure 1). To further assign this band, we conducted isotopic labeling experiments with H_2O and $H_2{}^{18}O$. The lack of an isotopic shift when the solvent was switched from D_2O to H_2O implies that the vibrational mode of the species does not involve a hydrogen atom (Figure 2B). Upon switching to the $H_2{}^{18}O$ electrolyte, this band shifts to 966 cm^{-1} (Figure 2C). The 48 cm^{-1} difference (from 1,014 to 966 cm^{-1}) indicates that the intermediate involves an O-containing motif. These experimental

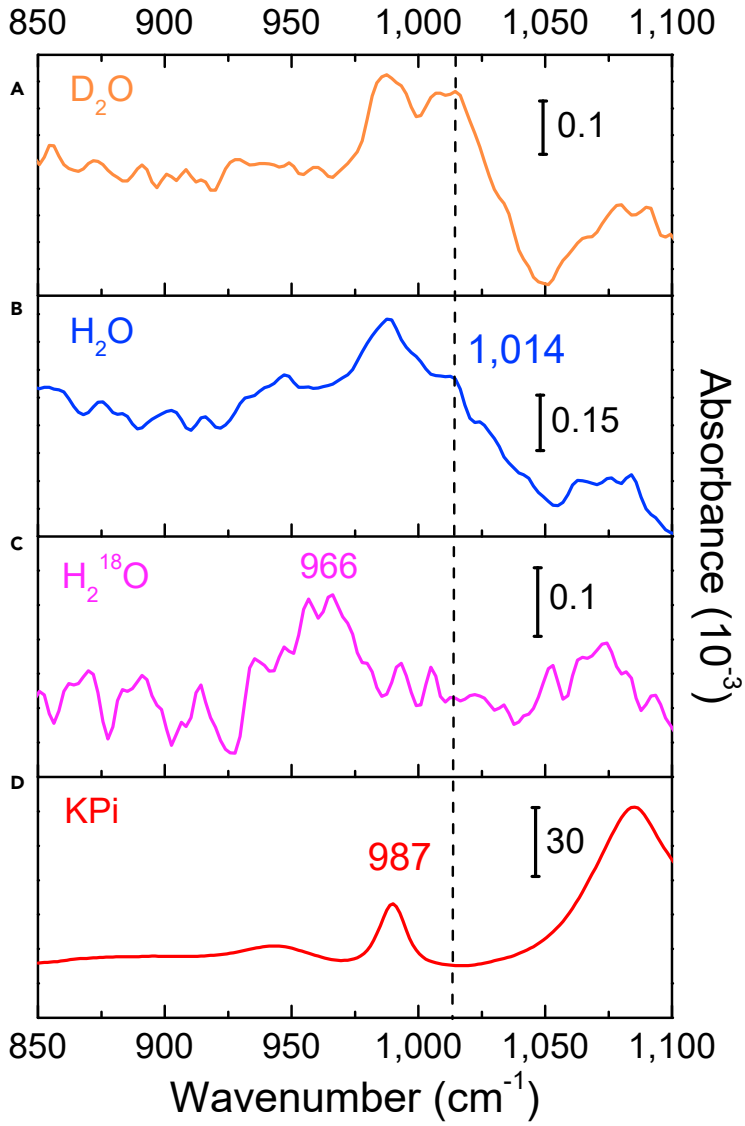

Figure 2. Observation of a superoxo intermediate by SEIRAS-ATR on a $CoO_x(OH)_y$-Au electrode
(A–C) Spectra collected on electrodes in contact with 0.1 M solutions of KPi in: (A) D_2O, (B) H_2O, and (C) $H_2{}^{18}O$ at a sample potential of 2.21 V. A spectrum at 1.61 V served as a reference spectrum. The band of the superoxo species is centered at 1,014 cm^{-1} in the presence of D_2O and H_2O and occurs at 966 cm^{-1} in the presence of $H_2{}^{18}O$. All other spectral changes are attributed to KPi.
(D) Spectrum of a bulk KPi solution.

observations support the conclusion that the 1,014 cm^{-1} band is associated with the superoxide intermediates (Co–O–O•–Co or Co–O–O•).[13,43,53] The other possible water-oxidation intermediate, hydroperoxide (Co–O–OH), would feature characteristic bands in the 740–920 cm^{-1} region.[42,44,54,55] Owing to the absorption by the H_2O librational mode, the signals were too weak to be discernable in that spectral range. The other bands in the spectra in Figures 2A–2C are due to the enrichment and depletion of electrolyte phosphate species at the interface with changes in applied potential. The magnitude of those spectral changes depends on the characteristics of a specific electrode, such as film thickness and homogeneity, and the electrolyte system. The negative band at ~1,050 cm^{-1} in Figures 2A and 2B is likely

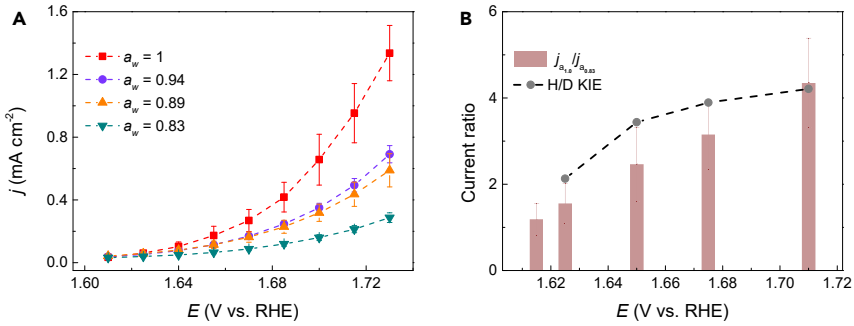

Figure 3. Potential dependence of the current modulation ratio for different water activities and solvents

(A) Suppression of the current density due to the water-oxidation reaction on Co–Pi when a_w was decreased from 1 to 0.83. The water activity was altered by setting the $NaNO_3$ concentration in a 0.1 M KPi buffer at neutral pH to 0, 2, 4, and 7 m. The data were collected on a Co–Pi film on an FTO substrate under steady-state conditions and under stirring of the electrolyte. The data were derived from an average of three independent experiments for each a_w. Error bars denote the standard deviation of three individual measurements. The potential was corrected for the *iR*-drop. Further experimental details are provided in the supplemental information.

(B) $j_{a1.0}/j_{a0.83}$ is the ratio of the water-oxidation current densities on the Co–Pi catalyst observed in electrolytes with water activities of 1 and 0.83. The ratio $j_{a1.0}/j_{a0.83}$ was calculated from the data in Figure 3A. H/D refers to the ratio of the current densities of the Co–Pi catalyst in 0.1 M KPi in H_2O and D_2O.

due to a surface-adsorbed phosphate species.[56,57] The spectrum of a bulk KPi solution is shown in Figure 2D. Duplicate experiments confirm the reproducibility of the spectroscopic results (Figure S5). Taken together, this set of experiments demonstrates the utility of the SEIRAS-ATR technique for the detection of water-oxidation intermediates under operating conditions. Importantly, the result confirms the presence of a superoxo species, consistent with the mechanistic proposal (Figure 1). Future research should be directed to further distinguish between Co–O–O$^{\bullet}$–Co and Co–O–O$^{\bullet}$.

Electrochemical characterization with varying water activities

To further probe the mechanisms as shown in Figure 1, we monitored the electrochemical water oxidation current as a function of electrode potential in water-in-salt electrolytes of varying water activities. As noted earlier, different reaction orders with respect to water activity are expected from the two competing mechanisms: a (pseudo) first-order dependence on H_2O activity (a_w) is expected for the WNA route, whereas a (pseudo) zeroth-order dependence on a_w is expected for the IMOC pathway. In a practical electrochemical system, the dependence of the kinetics on a_w is likely more complicated because of a number of other factors, including the participation of H_2O as a solvent; these potential complications notwithstanding, the value of quantitatively analyzing the reaction rates as a function of water activity becomes obvious.

Figure 3A compares the steady-state electrochemical current densities due to the oxidation of water on Co–Pi in contact with 0.1 M KPi containing 0, 2, 4, and 7 m $NaNO_3$. The corresponding water activities are shown in the legend and were calculated on the basis of empirical equations.[58] These values describe the activity of bulk water in these water-in-salt electrolytes. We caution that the activity of water at the electrocatalytic interface may be different from those values. Nevertheless, the activities of interfacial water are expected to qualitatively follow the same

trend with increasing water-in-salt concentration. All electrolytes were at neutral pH and were stirred during measurements, which were performed on electrodeposited Co–Pi on fluorine-doped tin oxide (FTO) substrates in a single-compartment electrochemical cell. The potential window was carefully chosen so as to avoid mass transport limitations (i.e., >1.71 V) or large experimental errors due to low current densities (i.e., <1.62 V). Details of the data collection protocol are given in the supplemental information, and a representative dataset is shown in Figure S6. As shown, with increasing molality of $NaNO_3$ and, hence, decreasing a_w, the current density of water oxidation is increasingly suppressed. A similar trend was observed for $CoO_x(OH)_y$ (Figure S7), suggesting that the observed trend is a more general feature of cobalt oxide-based catalysts. This finding further corroborates our assertion made earlier that $CoO_x(OH)_y$ is an appropriate alternative model system for Co–Pi.

The observed suppression of the water-oxidation reaction could arise from a number of different physical phenomena. First, to test whether the catalyst undergoes irreversible structural changes in the different electrolytes, we recorded the cyclic voltammograms (CVs) of the same Co–Pi electrode in 0.1 M KPi before and after collection of 3 cycles of CVs in the four electrolytes (of molalities 0, 2, 4, and 7 m). As shown in Figure S8, the CVs in 0.1 M KPi before and after catalysis in the water-in-salt electrolytes overlap. These data suggest that no irreversible changes in catalytic activity occur during water oxidation in the water-in-salt electrolytes.

Second, to test whether the mass transport of water to the electrode limits the reaction rate at high salt concentrations, we collected the steady-state electrochemical current densities of a Co–Pi-coated Pt rotating disk electrode (RDE) at rotation rates of 2,000 rpm (Figure S9) and 0 rpm (Figure S10). Comparison of the two figures reveals that the recorded current densities on the RDE exhibit the same trend with increasing salt concentration, irrespective of the rotation rate. Moreover, as demonstrated in Table S1, the increase in the thickness of the stagnant layer with electrolyte concentration is expected to be small. Collectively, these results suggest that the suppression of the water-oxidation reaction is not caused by limited mass transport of water to the electrode.

Third, at high concentrations of $NaNO_3$, nitrate anions are expected to limit the enrichment of phosphate anions in the electric double layer with increasing potential. As a result, the pH buffer capacity at the electrocatalytic interface might decrease with increasing $NaNO_3$ concentration. Changes in the pH in the vicinity of the electrode (local pH) could impact the reaction rate and mechanism.[27,59] To exclude local pH effects as a possible reason for the reactivity trends with increasing $NaNO_3$ concentration, we performed three different control experiments: (1) we monitored the electrochemical current density as a function of solution pH at a fixed (absolute) electrode potential. As shown in Figures S11–S13, the pH dependence of the current density was independent of the rotation rate of the RDE. (2) We performed galvanostatic titration experiments. The potential shows an approximately Nernstian shift of 60 mV/pH for all electrolytes (Figures S11–S13). (3) We varied the concentration of KPi in the electrolytes containing 4 and 7 m $NaNO_3$. As shown in Figure S14, the potential dependence of the reaction rate is insensitive to the concentration of KPi. Taken together, these control experiments suggest that the local pH does not significantly depend on the concentration of $NaNO_3$.

Fourth, to test whether nitrate anions block catalytic sites, we recorded the electrochemical current density as a function of potential in 7 m $NaClO_4$. Perchlorate

typically does not chemisorb on electrodes.[60] As shown in Figure S15, the impact of 7 m $NaClO_4$ on the current density is similar to that of 7 m $NaNO_3$. This result indicates that nitrate anions do not block catalytic sites of Co–Pi.

Fifth, alkali metal cations are known to influence the rate of the water-oxidation reaction on various electrocatalysts.[61–65] In the case of Ni oxyhydroxides, intercalated electrolyte cations have been proposed to stabilize reaction intermediates.[62,64] To test whether the catalytic activity is affected by the identity of the cation, we conducted additional control experiments in 2 m KNO_3. As shown in Figure S16, the current modulation ratio virtually overlaps with the one obtained in 2 m $NaNO_3$ (higher concentrations of KNO_3 could not be tested because of the lower solubility of that salt relative to $NaNO_3$). This result is consistent with earlier work[66] showing that the substitution of K^+ in Co–Pi by Na^+ has no significant impact on the catalytic activity of this catalyst. On the basis of this finding and our observation that the catalytic activity of Co–Pi is retained after a sequence of CVs in three water-in-salt electrolytes (Figure S8), we can exclude the incorporation of Na^+ into the Co–Pi film as the origin of the change in catalytic activity with increasing electrolyte concentration. Cations can also influence an electrocatalytic process by altering the properties of the electric double layer in a number of distinct ways,[67] which are not fully understood to date. One of the principal ways in which cations can impact the catalytic activity is by altering the structure and dynamics of water at the interface.[65,67] This possibility is included in our interpretation of these results in terms of the decreasing activity of water with increasing concentration of the water-in-salt electrolytes.

Sixth, to exclude the possibility that impurities, for example, Fe, incorporate into the catalyst[68] with increasing salt concentration, we performed CV tests in electrolytes with reagent grade and trace metal grade salts. As shown in Figure S17, the same water-oxidation activity was observed in both electrolytes.

Finally, to test whether the electrochemical currents arise from the oxidation of water to molecular oxygen, we conducted gas chromatography measurements. Figure S18 shows that O_2 is produced with near-unity faradaic efficiency. This measurement demonstrates that: (1) other possible oxidation products (such as H_2O_2) are not produced in appreciable amounts and (2) parasitic chemical reactions (such as the oxidation of nitrate) do not occur.

Taken as a whole, this set of results indicates that the observed suppression of the water-oxidation reaction is most likely caused by the decrease of water activity (a_w) from 1 to 0.83 as the concentration of $NaNO_3$ increases from 0 to 7 m.

To further analyze the data shown in Figure 3A, we plotted the ratio of the current density at $a_w = 1$ over that at $a_w = 0.83$ at different potentials (Figure 3B). This ratio quantifies the extent to which the reaction rate is modulated by the water activity. It is clear that the impact of the water activity strongly depends on the electrode potential: at 1.71 V, the rate is suppressed by a factor of ≈ 4.3. By contrast, at a potential of 1.615 V, the modulation factor is only ≈ 1.2, indicating that the rate of the reaction is less sensitive to the change in water activity at that potential. Identical trends were obvious for the other a_w's (i.e., 0.94 and 0.89), albeit with different magnitudes.

That the reaction rate is suppressed by up to a factor of 4.3 by an a_w change from 1 to 0.83 at 1.71 V strongly suggests that H_2O is involved in the RDS at that potential. Conversely, for the same a_w, the modulation is close to unity at 1.615 V, indicating that H_2O involvement in the RDS is less likely. Taken as a whole, the data suggest

that a mechanistic switch occurs between 1.615 and 1.71 V. A possible mechanistic switch that is consistent with our observations is the transition from the IMOC pathway ([pseudo] zeroth order in a_w) to the WNA route ([pseudo] first order in a_w) as the electrode potential is increased from 1.615 to 1.71 V.

To corroborate further this assertion, we measured the steady-state current density on the FTO-supported Co–Pi electrode in 0.1 M KPi in heavy water (D_2O) as a function of electrode potential. The ratio of the current density of the corresponding measurement in light water over that in heavy water is the apparent kinetic isotope effect (KIE). The apparent KIE is close to 2 at 1.625 V and increases to $\approx$4.2 as the potential is tuned to 1.71 V. Because the IMOC pathway does not involve water in the RDS, we expect the rate of the reaction to be insensitive to H/D substitution. By contrast, the WNA involves a water molecule in the RDS. Therefore, a dependence of the rate on the isotope of hydrogen is expected. Collectively, the KIE measurements further corroborate our notion that the mechanism switches from the IMOC route to the WNA pathway with increasing potential.

We note that the interpretation of KIE effects can be highly complex. For example, a similar KIE dependence on potential might be explained by a switch of the oxidized substrates from OH^- to H_2O, as has been reported by Zhao et al. on Fe_2O_3.[69] However, that mechanism is not applicable to the Co–Pi catalyst because OH^- is unlikely to be the oxidized substrate at pH 7. Furthermore, Hammes-Schiffer et al. demonstrated that the relative contributions that specific reactant/product vibronic states make to the current density are dependent on the isotope.[70] They showed that this effect could give rise to a potential dependence of the KIE. Although we cannot fully rule out that such effects contribute to the potential dependence of the KIE in the present case, the corroboration between the KIE data and the potential-dependent impact of the water activity on the reaction rate supports the conclusion of a potential-induced switch from the IMOC mechanism to the WNA pathway with increasing potential. A KIE on the WNA pathway was also reported by Cuk et al. during the photocatalytic oxidation of water on $SrTiO_3$.[18]

As far as the KIE effect is concerned, it is noted that Dau and co-workers also found a suppression of the water-oxidation reaction in D_2O relative to that in H_2O.[32] Their electrokinetic results were similar to those reported herein. However, they interpreted these data differently. In particular, the authors found that the redox potential of the pre-equilibrium $[Co^{III}–OH] \leftrightharpoons [Co^{IV}–O] + H^+ + e^-$ shifts by approximately 60 mV in the anodic direction upon switching the solvent from H_2O to D_2O. Because galvanostatic measurements for water oxidation in H_2O and D_2O show a similar shift, they suggested that the suppression of the water-oxidation reaction is due to the shift in this pre-equilibrium (rather than a KIE on the RDS of the water-oxidation reaction). This pre-equilibrium is a critical factor determining the activity of Co-oxide-based catalysts.[27,31,71] This alternative interpretation could also account for the observed suppression of the water oxidation in D_2O. However, we note that on the basis of the CVs of Co–Pi in H_2O and D_2O (Figure S19), we estimated a shift of $\approx$28 mV in the Co(II)/Co(III) redox half-wave potential. The relatively small shift in the pre-equilibrium suggests that it may not be the sole reason for the observed dependence of the rate of the water oxidation on the H/D isotope. Most importantly, this interpretation cannot account for the suppression of the current with increasing salt concentration (Figure 3). As discussed earlier, our control experiments in which we varied the rotation rate of the RDE (Figures S9 and S10), the pH of the electrolyte (Figures S11–S13), and the concentration of KPi (Figure S14) confirm that the buffer capacity is sufficient to maintain the $[Co^{III}–OH] \leftrightharpoons [Co^{IV}–O] + H^+ + e^-$ equilibrium in

the water-in-salt electrolytes. To further corroborate this notion, we analyzed the Co(II)/Co(III) redox equilibrium of Co–Pi in contact with the water-in-salt electrolytes with cyclic voltammetry. As shown in Figure S20, the Co(II)/Co(III) redox half-wave potential is shifted by only 10–20 mV in the cathodic direction with increasing salt concentration. This small shift indicates the pre-equilibrium is not significantly affected by the presence of water-in-salt electrolytes. Therefore, when the isotope effect results are viewed in the context of the electrokinetic results for the water-in-salt electrolytes, our interpretation provides a cohesive, self-consistent picture, whereas the hypothesis of the shift in the pre-equilibrium can only partly explain the collective results. Although the shift may be a contributing factor, we conclude that it is not the dominating effect.

Rationalization of the potential-induced mechanistic switch

In the following section, we discuss two possible molecular origins for our proposed potential-induced mechanistic switch. First, we show that the interfacial electric field at the electrocatalyst/electrolyte contact may affect the relative activation barriers of the two pathways and, thus, the relative weight of each route as the potential is altered. Second, we performed a DFT study of the two routes. These calculations show that only at high potentials does the WNA mechanism become thermodynamically accessible. In a practical system, the two effects may synergistically combine to favor the WNA pathway at high electrode potentials. Next, we discuss the impact of the interfacial electric field on the activation barriers; then we describe the insights derived from the DFT modeling.

The key distinction between the IMOC and WNA pathways is the involvement of water in the RDS of the latter one (Figure 1). On the basis of this observation, we expect the energetics of the two pathways to exhibit distinct sensitivity to the interfacial electric field. The magnitude of the interfacial electric field of the electric double layer increases as the potential of the electrode is increased. It is well established that electric fields can profoundly impact the rates and selectivity of chemical reactions.[72–76] Reaction intermediates with sufficiently large dipole moments and polarizabilities can interact with the electric fields. As a result of this interaction, the free energy profile of the reaction processes can be altered.[72,73] Nørskov et al. have shown that the impact of electric fields on surface-bound water-oxidation intermediates (M–OOH, M–OH, M=O) is typically very small because these species have small dipole moments and polarizabilities.[75] On the basis of these findings, it is likely that the interfacial electric field has a negligible impact on the IMOC pathway. Because the rate-determining O–O bond-formation step is a chemical step, we expect the principal activation barrier of the IMOC pathway to be independent of the electrode potential. By contrast, because water has a relatively large dipole moment and polarizability, the orientation and dynamics of water molecules at electrified interfaces may strongly depend on the electrode potential.[76–78] It has been suggested that the water dynamics and structure at interfaces affect the rates of various electrocatalytic processes, such as water oxidation and reduction.[65,76] Therefore, even though O–O coupling in the WNA as hypothesized in Figure 1 is a chemical step, we expect the activation barrier of this process to depend on the electrode potential: $\Delta G^{\neq}_{WNA} = \Delta G^{\neq}_{WNA} - \Delta\vec{\mu}\cdot\vec{E}$, where $\Delta G^{\neq}_{WNA}$ is the standard chemical free energy of activation in the absence of an electric field; $\Delta\vec{\mu}$ represents the change in the surface dipole when going from the reactant to the activated complex state; and $\vec{E}$ is the interfacial electric field, which depends on the electrode potential. These qualitative considerations show that because of the participation of water in the rate-determining chemical step of O–O bond formation for the WNA mechanism, the activation barrier of this step is a function of electrode potential. Nevertheless,

without knowledge of the molecular-level structure of the electrocatalyst/electrolyte interface at the present time, our considerations must remain qualitative at the present stage. Irrespective, this model describes one possible origin of the observed mechanistic switch from the IMOC route to the WNA pathway with increasing potential.

To explore further other possible causes of the potential-induced switch, we studied the energetics of the two pathways with DFT. All calculations were performed with the B3LYP functional and def2-SV(P) and def2-TZVP basis set implemented in the Gaussian 16 software package. Further computational details are provided in the supplemental information. We constructed atomic models on the basis of previous EXAFS[34] and X-ray pair distribution function analysis.[52] The $Co_7O_{24}H_{27}$ cluster has a Co ion surrounded by 6 Co ions at the edge that are connected to the center Co ion by μ_3-O bridges (Figure S21). The energetics of the water-oxidation reaction is sensitive to the protonation state of the cluster.[35,36] We considered different protonation states and found that the lowest energy protonation state is a highly symmetric cluster with one side of the μ_3-O being protonated and each pair of edge Co ions having strong hydrogen bonds between nearby hydroxide and water ligands (Figure S22). The protonation of the hydroxide ligand of the edge Co atoms is energetically unfavorable because it destroys the strong hydrogen bond interaction between OH^- and nearby H_2O. However, the edge OH^- group can be protonated by reducing the corresponding edge Co(III) to Co(II) (Figure S23).

On the basis of this structural model, we investigated the water-oxidation mechanism (Figure 4) starting from the H_2O–Co(II)–$(\mu$-O$)_2$–Co(III)–OH_2 intermediates (I). We note that our computational method overestimates the potential for oxidation potential of Co(III) to Co(IV) by ~0.3 V (Figure S24). All potentials quoted herein are not corrected for this systematic error. The oxidation of Co(II) to Co(III) requires 0.95 V, which is much lower than the applied potential during catalysis. The second oxidation requires 1.98 V to generate intermediate III with one Co oxidized to Co(IV). This oxidation is a metal-center oxidation, consistent with X-ray absorption near edge structure results of the Co–Pi catalyst under catalytic conditions, which suggest a valence of Co greater than 3.[34] When the overestimation of the redox potential is accounted for, this intermediate is predicted to be prevalent under water-oxidation conditions. Consistent with the prediction, the resting state of the catalyst has been assigned to intermediate III in previous reports.[15,27,31,32,59,79] The hydroxide coordinated to the Co(IV) center in intermediate III has a partial radical character as indicated by a Mulliken spin population of 0.21 (Figure S25). Therefore, the two hydroxides can couple to form hydroperoxide through the IMOC mechanism. Thermodynamically, this pathway is favored over the WNA pathway under low applied potentials. The following two oxidations require low potentials. Therefore, it is fairly easy to form intermediate VI. The release of O_2 and binding of two water molecules complete the catalytic cycle.

Under high applied potential, intermediate III can be further oxidized to form intermediate IV′ with two nearby Co being oxidized to Co(IV). The terminal O atom coordinated to Co(IV) is best described as an oxyl radical because the Mulliken spin population on the O atom is 0.89 (Figure S25), close to 1 for a perfect radical. The intermediate IV′ can react with a water molecule from the solution to form intermediate V′ through the WNA mechanism. The incoming H_2O forms hydroperoxide with the oxyl radical and releases a proton to the nearby OH^- group. Intermediate V′ can be further oxidized to intermediate VI′, which releases O_2 and adsorbs a water molecule to complete the catalytic cycle.

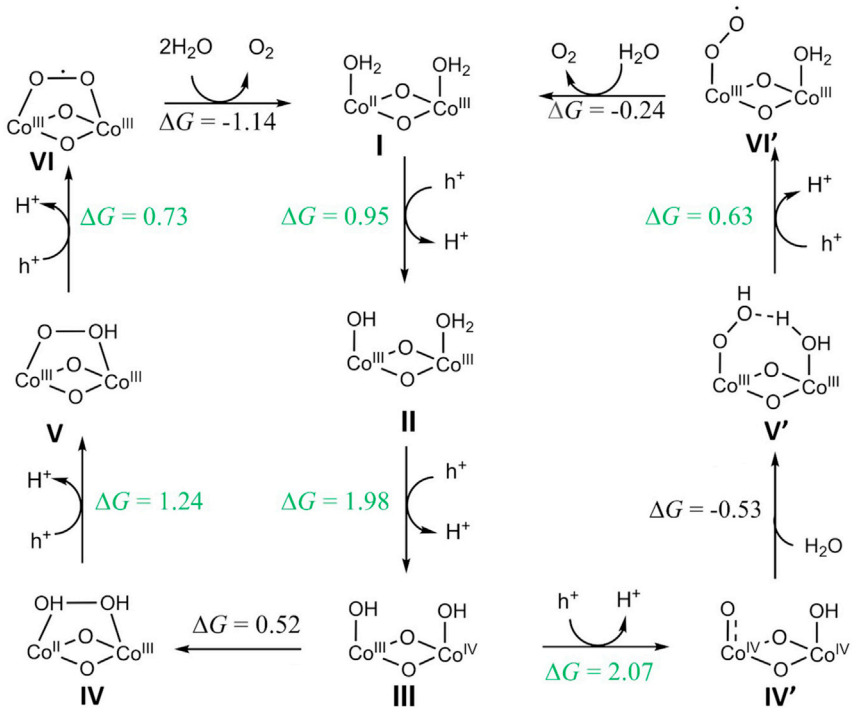

Figure 4. Possible routes of water oxidation suggested by the DFT calculations

Left: the IMOC mechanism under low overpotential (thermodynamically favored pathway); right: the WNA mechanism under high overpotential. The calculated free energy changes (ΔG) are given in the unit of eV. The numbers shown in green are the free energy changes of electrochemical steps versus the computed hydrogen electrode.

We note that both IMOC and WNA mechanisms feature a superoxo intermediate (VI and VI′, respectively). This prediction is consistent with our spectroscopic results, which indicate the presence of a superoxo species. On the basis of the simulated O–O vibrational frequencies (Figure S26) alone, we cannot identify which of the two species gives rise to the vibrational band at 1,014 cm^{-1} (Figure 2). We reserve a more detailed assignment for future investigations.

Although alternative reaction pathways may be available,[36,80] the DFT computations show that: (1) the IMOC and WNA pathways are feasible from a thermodynamic perspective and (2) their energetics are consistent with the proposed mechanistic framework (Figure 1) and the interpretation of our electrokinetic results (Figure 3); at low overpotential, the IMOC pathway predominates, whereas the WNA pathway becomes accessible at high overpotential. Finally, it is noted that, in line with previous precedence, we only considered the thermodynamics of the pathways.[19,80] The calculation of the activation barriers is complicated by spin-state changes during the conversion of intermediate III to IV. Furthermore, the activation barriers are sensitive to the protonation state of the catalyst, which is a complex function of applied electrode potential and reaction conditions. Fully accounting for these complications will require additional research that is beyond of the scope of the current work.

Taken as a whole, the thermodynamic description of the two pathways and the qualitative considerations of the impact of the interfacial field on the relative magnitude of activation barriers of the O–O bond-forming steps provide strong support for the conclusion of a potential-dependent mechanistic switch. The DFT modeling predicts that a certain threshold potential for the WNA pathway needs to be surpassed

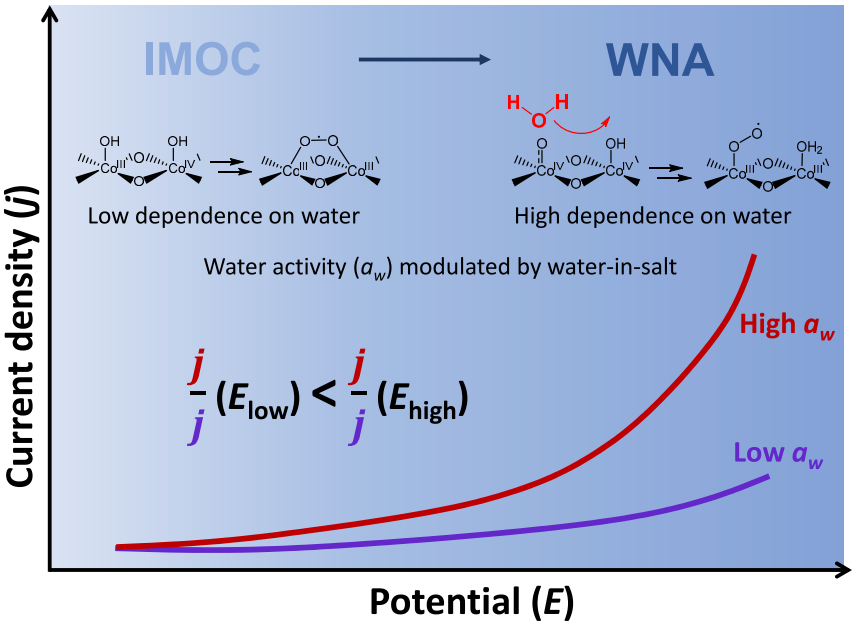

Figure 5. Schematic representation of the key findings and conclusions of this work

before this pathway becomes thermodynamically feasible. In addition, the involvement of water in the RDS may further lower the activation barrier for the O–O bond-formation step for the WNA route, leading to a further acceleration of the reaction rate. Our conclusions are graphically summarized in Figure 5.

Broader implications

Previous research on homogeneous water-oxidation mechanisms has revealed that the 4-proton, 4-electron process of water oxidation can take place on a mononuclear or a dinuclear catalyst. Whether WNA or oxygen coupling is the preferred mechanism has been at the center of intense studies for the natural PSII and for molecular catalysts. In testing the various hypotheses for the reaction mechanisms, researchers mainly relied on kinetic models that depend on the information of key species, such as the concentration of the catalyst and the TOFs. In principle, the same methodology could be applied for the establishment of a similar knowledge base for heterogeneous water-oxidation reactions. However, the lack of knowledge on the detailed information of the catalytically active centers creates a critical challenge for such an approach. Our strategy of probing the kinetics of heterogeneous water oxidation by varying water activities is new. It generates information that permits the verification of hypotheses that are difficult or impossible to obtain by other methods. How the water-oxidation reaction proceeds is sensitive to a number of factors, including the local catalytic environment (e.g., the availability of mononuclear, dinuclear, or multinuclear active centers), substrate concentration, and the driving forces (see, e.g., a recent report on how varying applied potentials change water-oxidation products on a copper porphyrin in acidic solutions.[81]) Although our studies suggest that the WNA mechanism is favored at high driving force, we are inspired to understand that in a practical water-oxidation system (such as the oxygen evolution catalyst in PSII or in an electrolyzer), both mechanisms may co-exist. The fact that this switch is observed on Co–Pi and $CoO_x(OH)_y$ (Figures S7 and S27) suggests that the potential-induced changes in pathway may be a more general phenomenon of Co-oxide-based electrocatalysts. The dynamic switch of the mechanisms could help to explain how nature ensures the most efficient route for the utilization of solar

energy to liberate electrons and protons; it also implies that future designs and optimization of heterogeneous catalysts for large-scale engineering implementations of water oxidation should consider the facile switch of reaction mechanisms. It is noted that the WNA mechanism could proceed through a mononuclear site or a dinuclear site depending on the catalytic conditions.[13,82,83] However, it likely makes only a minor contribution to our study because of the narrow and low overpotential regime investigated and the equivalent involvement of a water molecule in the RDS on both sites. Finally, although we envision that studying water oxidation by varying water activities indeed adds a new dimension to the tool kit, it faces limitations for systems at highly alkaline conditions where OH^- but not H_2O is being oxidized.

In conclusion, this work introduced two key innovations. Using SEIRAS-ATR, we detected a key intermediate corresponding to O–O bond formation in Co-based water oxidation. This information lends support to the proposed mechanisms. By varying the water activity, we established a kinetic model that allowed us to verify the two competing mechanisms of water oxidation. We found that the dinuclear route (i.e., IMOC) is favored at relatively low driving forces, whereas the mononuclear route (i.e., WNA) is preferred at relatively high driving forces. The results contribute significantly to the understanding of water oxidation by heterogeneous catalysts.

EXPERIMENTAL PROCEDURES

Resource availability

Lead contact

Further information and requests for resources should be directed to and will be fulfilled by the Lead Contact, Dunwei Wang (dunwei.wang@bc.edu).

Materials availability

This study did not generate new unique reagents.

Data and code availability

This study did not generate any datasets.

SUPPLEMENTAL INFORMATION

Supplemental information can be found online at https://doi.org/10.1016/j.chempr.2021.03.015.

ACKNOWLEDGMENTS

The work at Boston College is supported by the U.S. Department of Energy (DOE), Office of Science, Office of Basic Energy Sciences, Chemical Sciences, Geosciences, and Biosciences Division (DE-SC0020261). Work at Yale University was supported by the U.S. Department of Energy (DOE), Office of Science, Office of Basic Energy Sciences, Chemical Sciences, Geosciences, and Biosciences Division (DE-FG02-07ER15909). V.S.B. acknowledges the computer time from the National Energy Research Scientific Computing Center (NERSC) and Yale Center for Research Computing (YCRC).

AUTHOR CONTRIBUTIONS

C.L. and Y.W. performed the electrochemical experiments; J.L. performed the SEIRAS-ATR experiments; K.R.Y. conducted computational studies; J.E.T., Q.D., D.H., and Y.Z. contributed experimentally; all authors participated in discussions and the writing of the manuscript; V.S.B., M.M.W., and D.W. co-directed the project.

DECLARATION OF INTERESTS

The authors declare no competing interests.

Received: November 2, 2020
Revised: January 13, 2021
Accepted: March 16, 2021
Published: April 14, 2021

REFERENCES

1. Shen, J.R. (2015). The structure of photosystem II and the mechanism of water oxidation in photosynthesis. Annu. Rev. Plant Biol. *66*, 23–48.

2. Vinyard, D.J., and Brudvig, G.W. (2017). Progress toward a molecular mechanism of water oxidation in photosystem II. Annu. Rev. Phys. Chem. *68*, 101–116.

3. Blakemore, J.D., Crabtree, R.H., and Brudvig, G.W. (2015). Molecular catalysts for water oxidation. Chem. Rev. *115*, 12974–13005.

4. Shaffer, D.W., Xie, Y., and Concepcion, J.J. (2017). O–O bond formation in ruthenium-catalyzed water oxidation: single-site nucleophilic attack vs. O–O radical coupling. Chem. Soc. Rev. *46*, 6170–6193.

5. Hunter, B.M., Gray, H.B., and Müller, A.M. (2016). Earth-abundant heterogeneous water oxidation catalysts. Chem. Rev. *116*, 14120–14136.

6. Suen, N.T., Hung, S.F., Quan, Q., Zhang, N., Xu, Y.J., and Chen, H.M. (2017). Electrocatalysis for the oxygen evolution reaction: recent development and future perspectives. Chem. Soc. Rev. *46*, 337–365.

7. Zhang, M., and Frei, H. (2017). Water oxidation mechanisms of metal oxide catalysts by vibrational spectroscopy of transient intermediates. Annu. Rev. Phys. Chem. *68*, 209–231.

8. Yu, Z.Y., Duan, Y., Gao, M.R., Lang, C.C., Zheng, Y.R., and Yu, S.H. (2017). A one-dimensional porous carbon-supported Ni/Mo_2C dual catalyst for efficient water splitting. Chem. Sci. *8*, 968–973.

9. Yu, Z.-Y., Lang, C.-C., Gao, M.-R., Chen, Y., Fu, Q.-Q., Duan, Y., and Yu, S.-H. (2018). Ni–Mo–O nanorod-derived composite catalysts for efficient alkaline water-to-hydrogen conversion via urea electrolysis. Energy Environ. Sci. *11*, 1890–1897.

10. Grimaud, A., Diaz-Morales, O., Han, B., Hong, W.T., Lee, Y.L., Giordano, L., Stoerzinger, K.A., Koper, M.T.M., and Shao-Horn, Y. (2017). Activating lattice oxygen redox reactions in metal oxides to catalyse oxygen evolution. Nat. Chem. *9*, 457–465.

11. Negahdar, L., Zeng, F., Palkovits, S., Broicher, C., and Palkovits, R. (2019). Mechanistic aspects of the electrocatalytic oxygen evolution reaction over Ni–Co oxides. ChemElectroChem *6*, 5588–5595.

12. Zandi, O., and Hamann, T.W. (2016). Determination of photoelectrochemical water oxidation intermediates on haematite electrode surfaces using operando infrared spectroscopy. Nat. Chem. *8*, 778–783.

13. Zhang, M., de Respinis, M., and Frei, H. (2014). Time-resolved observations of water oxidation intermediates on a cobalt oxide nanoparticle catalyst. Nat. Chem. *6*, 362–367.

14. Rosenthal, J., and Nocera, D.G. (2007). Role of proton-coupled electron transfer in O–O bond activation. Acc. Chem. Res. *40*, 543–553.

15. Ullman, A.M., Brodsky, C.N., Li, N., Zheng, S.L., and Nocera, D.G. (2016). Probing edge site reactivity of oxidic cobalt water oxidation catalysts. J. Am. Chem. Soc. *138*, 4229–4236.

16. Romain, S., Vigara, L., and Llobet, A. (2009). Oxygen–oxygen bond formation pathways promoted by ruthenium complexes. Acc. Chem. Res. *42*, 1944–1953.

17. García-Melchor, M., Vilella, L., López, N., and Vojvodic, A. (2016). Computationally probing the performance of hybrid, heterogeneous, and homogeneous iridium-based catalysts for water oxidation. ChemCatChem *8*, 1792–1798.

18. Chen, X., Aschaffenburg, D.J., and Cuk, T. (2019). Selecting between two transition states by which water oxidation intermediates decay on an oxide surface. Nat. Catal. *2*, 820–827.

19. Craig, M.J., Coulter, G., Dolan, E., Soriano-López, J., Mates-Torres, E., Schmitt, W., and García-Melchor, M. (2019). Universal scaling relations for the rational design of molecular water oxidation catalysts with near-zero overpotential. Nat. Commun. *10*, 4993.

20. Matheu, R., Ertem, M.Z., Gimbert-Suriñach, C., Sala, X., and Llobet, A. (2019). Seven coordinated molecular ruthenium–water oxidation catalysts: a coordination chemistry journey. Chem. Rev. *119*, 3453–3471.

21. Duan, L., Bozoglian, F., Mandal, S., Stewart, B., Privalov, T., Llobet, A., and Sun, L. (2012). A molecular ruthenium catalyst with water-oxidation activity comparable to that of photosystem II. Nat. Chem. *4*, 418–423.

22. Romain, S., Bozoglian, F., Sala, X., and Llobet, A. (2009). Oxygen–oxygen bond formation by the Ru-Hbpp water oxidation catalyst occurs solely via an intramolecular reaction pathway. J. Am. Chem. Soc. *131*, 2768–2769.

23. Le Formal, F., Pastor, E., Tilley, S.D., Mesa, C.A., Pendlebury, S.R., Grätzel, M., and Durrant, J.R. (2015). Rate law analysis of water oxidation on a hematite surface. J. Am. Chem. Soc. *137*, 6629–6637.

24. Zhao, Y., Yan, X., Yang, K.R., Cao, S., Dong, Q., Thorne, J.E., Materna, K.L., Zhu, S., Pan, X., Flytzani-Stephanopoulos, M., et al. (2018). End-on bound iridium dinuclear heterogeneous catalysts on WO_3 for solar water oxidation. ACS Cent. Sci. *4*, 1166–1172.

25. Zhao, Y., Yang, K.R., Wang, Z., Yan, X., Cao, S., Ye, Y., Dong, Q., Zhang, X., Thorne, J.E., Jin, L., et al. (2018). Stable iridium dinuclear heterogeneous catalysts supported on metal-oxide substrate for solar water oxidation. Proc. Natl. Acad. Sci. USA *115*, 2902–2907.

26. Wuttig, A., Yoon, Y., Ryu, J., and Surendranath, Y. (2017). Bicarbonate is not a general acid in Au-catalyzed CO_2 electroreduction. J. Am. Chem. Soc. *139*, 17109–17113.

27. Surendranath, Y., Kanan, M.W., and Nocera, D.G. (2010). Mechanistic studies of the oxygen evolution reaction by a cobalt-phosphate catalyst at neutral pH. J. Am. Chem. Soc. *132*, 16501–16509.

28. Suo, L., Borodin, O., Gao, T., Olguin, M., Ho, J., Fan, X., Luo, C., Wang, C., and Xu, K. (2015). "Water-in-salt" electrolyte enables high-voltage aqueous lithium-ion chemistries. Science *350*, 938–943.

29. Dong, Q., Yao, X., Zhao, Y., Qi, M., Zhang, X., Sun, H., He, Y., and Wang, D. (2018). Cathodically stable Li-O_2 battery operations using water-in-salt electrolyte. Chem *4*, 1345–1358.

30. Dong, Q., Zhang, X., He, D., Lang, C., and Wang, D. (2019). Role of H_2O in CO_2 electrochemical reduction as studied in a water-in-salt system. ACS Cent. Sci. *5*, 1461–1467.

31. Bergmann, A., Jones, T.E., Martinez Moreno, E., Teschner, D., Chernev, P., Gliech, M., Reier, T., Dau, H., and Strasser, P. (2018). Unified structural motifs of the catalytically active state of Co(oxyhydr)oxides during the electrochemical oxygen evolution reaction. Nat. Catal. *1*, 711–719.

32. Pasquini, C., Zaharieva, I., González-Flores, D., Chernev, P., Mohammadi, M.R., Guidoni, L., Smith, R.D.L., and Dau, H. (2019). H/D isotope effects reveal factors controlling catalytic activity in Co-based oxides for water oxidation. J. Am. Chem. Soc. *141*, 2938–2948.

33. Kanan, M.W., and Nocera, D.G. (2008). In situ formation of an oxygen-evolving catalyst in neutral water containing phosphate and Co^{2+}. Science *321*, 1072–1075.

34. Kanan, M.W., Yano, J., Surendranath, Y., Dincă, M., Yachandra, V.K., and Nocera, D.G. (2010). Structure and valency of a cobalt–phosphate water oxidation catalyst determined by in situ X-ray spectroscopy. J. Am. Chem. Soc. *132*, 13692–13701.

35. Li, X., and Siegbahn, P.E.M. (2013). Water oxidation mechanism for synthetic Co–oxides with small nuclearity. J. Am. Chem. Soc. *135*, 13804–13813.

36. Wang, L.-P., and Van Voorhis, T. (2011). Direct-coupling O_2 bond forming a pathway in cobalt oxide water oxidation catalysts. J. Phys. Chem. Lett. *2*, 2200–2204.

37. McAlpin, J.G., Stich, T.A., Casey, W.H., and Britt, R.D. (2012). Comparison of cobalt and manganese in the chemistry of water oxidation. Coord. Chem. Rev. *256*, 2445–2452.

38. Mattioli, G., Giannozzi, P., Amore Bonapasta, A., and Guidoni, L. (2013). Reaction pathways for oxygen evolution promoted by cobalt catalyst. J. Am. Chem. Soc. *135*, 15353–15363.

39. Risch, M., Ringleb, F., Kohlhoff, M., Bogdanoff, P., Chernev, P., Zaharieva, I., and Dau, H. (2015). Water oxidation by amorphous cobalt-based oxides: in situ tracking of redox transitions and mode of catalysis. Energy Environ. Sci. *8*, 661–674.

40. Nakamura, R., and Nakato, Y. (2004). Primary intermediates of oxygen photoevolution reaction on TiO_2 (rutile) particles, revealed by in situ FTIR absorption and photoluminescence measurements. J. Am. Chem. Soc. *126*, 1290–1298.

41. Pavlovic, Z., Ranjan, C., van Gastel, M., and Schlögl, R. (2017). The active site for the water oxidising anodic iridium oxide probed through in situ Raman spectroscopy. Chem. Commun. (Camb) *53*, 12414–12417.

42. Sivasankar, N., Weare, W.W., and Frei, H. (2011). Direct observation of a hydroperoxide surface intermediate upon visible light-driven water oxidation at an Ir oxide nanocluster catalyst by rapid-scan FT-IR spectroscopy. J. Am. Chem. Soc. *133*, 12976–12979.

43. Zhang, Y., Zhang, H., Liu, A., Chen, C., Song, W., and Zhao, J. (2018). Rate-limiting O–O Bond formation pathways for water oxidation on hematite photoanode. J. Am. Chem. Soc. *140*, 3264–3269.

44. Liu, H., and Frei, H. (2020). Observation of O–O bond forming step of molecular Co_4O_4 cubane catalyst for water oxidation by rapid-scan FT-IR spectroscopy. ACS Catal *10*, 2138–2147.

45. Chen, X., Choing, S.N., Aschaffenburg, D.J., Pemmaraju, C.D., Prendergast, D., and Cuk, T. (2017). The formation time of Ti–O• and Ti–O•– Ti radicals at the n-$SrTiO_3$/Aqueous interface during photocatalytic water oxidation. J. Am. Chem. Soc. *139*, 1830–1841.

46. Herlihy, D.M., Waegele, M.M., Chen, X., Pemmaraju, C.D., Prendergast, D., and Cuk, T. (2016). Detecting the oxyl radical of photocatalytic water oxidation at an n-$SrTiO_3$/aqueous interface through its subsurface vibration. Nat. Chem. *8*, 549–555.

47. Yeo, B.S., and Bell, A.T. (2011). Enhanced activity of gold-supported cobalt oxide for the electrochemical evolution of oxygen. J. Am. Chem. Soc. *133*, 5587–5593.

48. Rao, R.R., Kolb, M.J., Giordano, L., Pedersen, A.F., Katayama, Y., Hwang, J., Mehta, A., You, H., Lunger, J.R., Zhou, H., et al. (2020). Operando identification of site-dependent water oxidation activity on ruthenium dioxide single-crystal surfaces. Nat. Catal. *3*, 516–525.

49. Osawa, M. (2001). Surface-enhanced infrared absorption. In Near-Field Optics and Surface Plasmon Polaritons, S. Kawata, ed. (Springer), pp. 163–187.

50. Miyake, H., Ye, S., and Osawa, M. (2002). Electroless deposition of gold thin films on silicon for surface-enhanced infrared spectroelectrochemistry. Electrochem. Commun. *4*, 973–977.

51. Morhart, T.A., Unni, B., Lardner, M.J., and Burgess, I.J. (2017). Electrochemical ATR-SEIRAS using low-cost, micromachined Si wafers. Anal. Chem. *89*, 11818–11824.

52. Du, P., Kokhan, O., Chapman, K.W., Chupas, P.J., and Tiede, D.M. (2012). Elucidating the domain structure of the cobalt oxide water splitting catalyst by X-ray pair distribution function analysis. J. Am. Chem. Soc. *134*, 11096–11099.

53. Diaz-Morales, O., Ferrus-Suspedra, D., and Koper, M.T.M. (2016). The importance of nickel oxyhydroxide deprotonation on its activity towards electrochemical water oxidation. Koper. Chem. Sci. *7*, 2639–2645.

54. Suzuki, M., Ishiguro, T., Kozuka, M., and Nakamoto, K. (1981). Resonance Raman spectra, excitation profiles, and infrared spectra of [N,N′-ethylenebis(salicylideniminato)]cobalt(II) in the solid state. Inorg. Chem. *20*, 1993–1996.

55. Jones, R.D., Summerville, D.A., and Basolo, F. (1979). Synthetic oxygen carriers related to biological systems. Chem. Rev. *79*, 139–179.

56. Klähn, M., Mathias, G., Kötting, C., Nonella, M., Schlitter, J., Gerwert, K., and Tavan, P. (2004). IR spectra of phosphate ions in aqueous solution: predictions of a DFT/MM approach compared with observations. J. Phys. Chem. A *108*, 6186–6194.

57. Tejedor-Tejedor, M.I., and Anderson, M.A. (1990). The protonation of phosphate on the surface of goethite as studied by CIR-FTIR and electrophoretic mobility. Langmuir *6*, 602–611.

58. Tang, I.N., and Munkelwitz, H.R. (1994). Water activities, densities, and refractive indices of aqueous sulfates and sodium nitrate droplets of atmospheric importance. J. Geophys. Res. *99*, 18801–18808.

59. Gerken, J.B., McAlpin, J.G., Chen, J.Y.C., Rigsby, M.L., Casey, W.H., Britt, R.D., and Stahl, S.S. (2011). Electrochemical water oxidation with cobalt-based electrocatalysts from pH 0–14: the thermodynamic basis for catalyst structure, stability, and activity. J. Am. Chem. Soc. *133*, 14431–14442.

60. Ronald Fawcett, W., and Ryan, P.J. (2010). Is perchlorate ion contact adsorbed from aqueous solutions at polarizable electrodes? J. Electroanal. Chem. *649*, 48–52.

61. Ding, C., Zhou, X., Shi, J., Yan, P., Wang, Z., Liu, G., and Li, C. (2015). Abnormal effects of cations (Li^+, Na^+, and K^+) on photoelectrochemical and electrocatalytic water splitting. J. Phys. Chem. B *119*, 3560–3566.

62. Garcia, A.C., Touzalin, T., Nieuwland, C., Perini, N., and Koper, M.T.M. (2019). Enhancement of oxygen evolution activity of nickel oxyhydroxide by electrolyte alkali cations. Angew. Chem. Int. Ed. Engl. *58*, 12999–13003.

63. Suntivich, J., Perry, E.E., Gasteiger, H.A., and Shao-Horn, Y. (2013). The influence of the cation on the oxygen reduction and evolution activities of oxide surfaces in alkaline electrolyte. Electrocatalysis *4*, 49–55.

64. Zaffran, J., Stevens, M.B., Trang, C.D.M., Nagli, M., Shehadeh, M., Boettcher, S.W., and Caspary Toroker, M. (2017). Influence of electrolyte cations on Ni(Fe)OOH catalyzed oxygen evolution reaction. Chem. Mater. *29*, 4761–4767.

65. Remsing, R.C., McKendry, I.G., Strongin, D.R., Klein, M.L., and Zdilla, M.J. (2015). Frustrated solvation structures can enhance electron transfer rates. J. Phys. Chem. Lett. *6*, 4804–4808.

66. Surendranath, Y., Dinca, M., and Nocera, D.G. (2009). Electrolyte-dependent electrosynthesis and activity of cobalt-based water oxidation catalysts. J. Am. Chem. Soc. *131*, 2615–2620.

67. Waegele, M.M., Gunathunge, C.M., Li, J., and Li, X. (2019). How cations affect the electric double layer and the rates and selectivity of electrocatalytic processes. J. Chem. Phys. *151*, 160902.

68. Trotochaud, L., Young, S.L., Ranney, J.K., and Boettcher, S.W. (2014). Nickel–iron oxyhydroxide oxygen-evolution electrocatalysts: the role of intentional and incidental iron incorporation. J. Am. Chem. Soc. *136*, 6744–6753.

69. Zhang, Y., Zhang, H., Ji, H., Ma, W., Chen, C., and Zhao, J. (2016). Pivotal role and regulation of proton transfer in water oxidation on hematite photoanodes. J. Am. Chem. Soc. *138*, 2705–2711.

70. Goldsmith, Z.K., Lam, Y.C., Soudackov, A.V., and Hammes-Schiffer, S. (2019). Proton discharge on a gold electrode from triethylammonium in acetonitrile: theoretical modeling of potential-dependent kinetic isotope effects. J. Am. Chem. Soc. *141*, 1084–1090.

71. Qi, J., Chen, M., Zhang, W., and Cao, R. (2019). Hierarchical-dimensional material: A $Co(OH)_2$ superstructure with hybrid dimensions for enhanced water oxidation. ChemCatChem *11*, 5969–5975.

72. Che, F., Gray, J.T., Ha, S., Kruse, N., Scott, S.L., and McEwen, J.-S. (2018). Elucidating the roles of electric fields in catalysis: a perspective. ACS Catal *8*, 5153–5174.

73. Chen, L.D., Urushihara, M., Chan, K., and Nørskov, J.K. (2016). Electric field effects in electrochemical CO_2 reduction. ACS Catal *6*, 7133–7139.

74. Gorin, C.F., Beh, E.S., Bui, Q.M., Dick, G.R., and Kanan, M.W. (2013). Interfacial electric field effects on a carbene reaction catalyzed by Rh porphyrins. J. Am. Chem. Soc. *135*, 11257–11265.

75. Karlberg, G.S., Rossmeisl, J., and Nørskov, J.K. (2007). Estimations of electric field effects on the oxygen reduction reaction based on the density functional theory. Phys. Chem. Chem. Phys. *9*, 5158–5161.

76. Ledezma-Yanez, I., Wallace, W.D.Z., Sebastián-Pascual, P., Climent, V., Feliu, J.M., and Koper, M.T.M. (2017). Interfacial water reorganization as a pH-dependent descriptor of the hydrogen evolution rate on platinum electrodes. Nat. Energy *2*, 17031.

77. Schultz, Z.D., Shaw, S.K., and Gewirth, A.A. (2005). Potential dependent organization of water at the electrified metal–liquid interface. J. Am. Chem. Soc. *127*, 15916–15922.

78. Toney, M.F., Howard, J.N., Richer, J., Borges, G.L., Gordon, J.G., Melroy, O.R., Wiesler, D.G., Yee, D., and Sorensen, L.B. (1994). Voltage-dependent ordering of water molecules at an electrode–electrolyte interface. Nature *368*, 444–446.

79. McAlpin, J.G., Surendranath, Y., Dinca, M., Stich, T.A., Stoian, S.A., Casey, W.H., Nocera, D.G., and Britt, R.D. (2010). EPR evidence for Co(IV) species produced during water oxidation at neutral pH. J. Am. Chem. Soc. *132*, 6882–6883.

80. Bajdich, M., García-Mota, M., Vojvodic, A., Nørskov, J.K., and Bell, A.T. (2013). Theoretical investigation of the activity of cobalt oxides for the electrochemical oxidation of water. J. Am. Chem. Soc. *135*, 13521–13530.

81. Liu, Y., Han, Y., Zhang, Z., Zhang, W., Lai, W., Wang, Y., and Cao, R. (2019). Low overpotential water oxidation at neutral pH catalyzed by a copper(II) porphyrin. Chem. Sci. *10*, 2613–2622.

82. Plaisance, C.P., and van Santen, R.A. (2015). Structure sensitivity of the oxygen evolution reaction catalyzed by cobalt(II,III) oxide. J. Am. Chem. Soc. *137*, 14660–14672.

83. Pham, H.H., Cheng, M.-J., Frei, H., and Wang, L.-W. (2016). Surface proton hopping and fast-kinetics pathway of water oxidation on Co_3O_4 (001) surface. ACS Catal *6*, 5610–5617.